Multidirection Piezoelectricity in Mono- and Multilayered Hexagonal α-In$_2$Se$_3$

Fei Xue,[†,‡,▼] Junwei Zhang,[†,▼] Weijin Hu,[§] Wei-Ting Hsu,[∥] Ali Han,[†] Siu-Fung Leung,[⊥] Jing-Kai Huang,[†] Yi Wan,[†] Shuhai Liu,[#] Junli Zhang,[†] Jr-Hau He,[⊥] Wen-Hao Chang,[∥] Zhong Lin Wang,[‡,¶] Xixiang Zhang,[*,†] and Lain-Jong Li[*,†,△]

[†]Physical Sciences and Engineering Division, King Abdullah University of Science and Technology, Thuwal 23955-6900, Saudi Arabia

[‡]Beijing Institute of Nanoenergy and Nanosystems, Chinese Academy of Sciences, Beijing 10083, China

[§]Shenyang National Laboratory for Materials Science, Institute of Metal Research (IMR), Chinese Academy of Sciences (CAS), Shenyang 110016, China

[∥]Department of Electrophysics, National Chiao Tung University, Hsinchu 30010, Taiwan

[⊥]Computer, Electrical, and Mathematical Sciences and Engineering Division, King Abdullah University of Science and Technology, Thuwal 23955-6900, Saudi Arabia

[#]School of Advanced Materials and Nanotechnology, Xidian University, Xian, Shaanxi 710071, China

[¶]School of Material Science and Engineering, Georgia Institute of Technology, Atlanta, Georgia 30332-0245, United States

[△]Corporate Research and Chief Technology Office, Taiwan Semiconductor Manufacturing Company (TSMC), Hsinchu 30075, Taiwan

S Supporting Information

ABSTRACT: Piezoelectric materials have been widely used for sensors, actuators, electronics, and energy conversion. Two-dimensional (2D) ultrathin semiconductors, such as monolayer h-BN and MoS$_2$ with their atom-level geometry, are currently emerging as new and attractive members of the piezoelectric family. However, their piezoelectric polarization is commonly limited to the in-plane direction of odd-number ultrathin layers, largely restricting their application in integrated nanoelectromechanical systems. Recently, theoretical calculations have predicted the existence of out-of-plane and in-plane piezoelectricity in monolayer α-In$_2$Se$_3$. Here, we experimentally report the coexistence of out-of-plane and in-plane piezoelectricity in monolayer to bulk α-In$_2$Se$_3$, attributed to their noncentrosymmetry originating from the hexagonal stacking. Specifically, the corresponding d_{33} piezoelectric coefficient of α-In$_2$Se$_3$ increases from 0.34 pm/V (monolayer) to 5.6 pm/V (bulk) without any odd−even effect. In addition, we also demonstrate a type of α-In$_2$Se$_3$-based flexible piezoelectric nanogenerator as an energy-harvesting cell and electronic skin. The out-of-plane and in-plane piezoelectricity in α-In$_2$Se$_3$ flakes offers an opportunity to enable both directional and nondirectional piezoelectric devices to be applicable for self-powered systems and adaptive and strain-tunable electronics/optoelectronics.

KEYWORDS: *multidirection, piezoelectricity, van der Waals crystal, monolayer and bulk, nanogenerator and electronic skin*
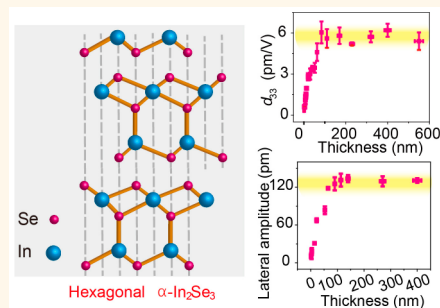
Piezoelectricity occurs in noncentrosymmetric materials including naturally formed crystals, artificial crystals, polymers, and biomolecules.[1−3] It has found extensive applications in sound production, energy conversion, sensors, and actuators.[1,4,5] The rapidly increasing demands for nanoscale and diverse functional piezoelectric devices drive researchers to explore low-dimensional piezoelectric materials. Theoretical efforts have predicted the in-plane piezoelectricity in various 2D layered structures including group II oxides, groups II−V compounds, and metal dichalcogenides.[6,7] Experimentally, 2D monolayer h-BN and transition metal dichalcogenides

(TMDCs) with structurally broken inversion symmetry have been reported to show only peculiar in-plane piezoelectricity along the e_{11} tensor direction,[8−11] limiting their applications in vertically integrated nanoelectromechanical systems. Moreover, unfortunately, the piezoelectricity of those 2D layered semi-conductors merely emerges in the atomic thickness level but gradually disappears with increasing thickness. Apart from the
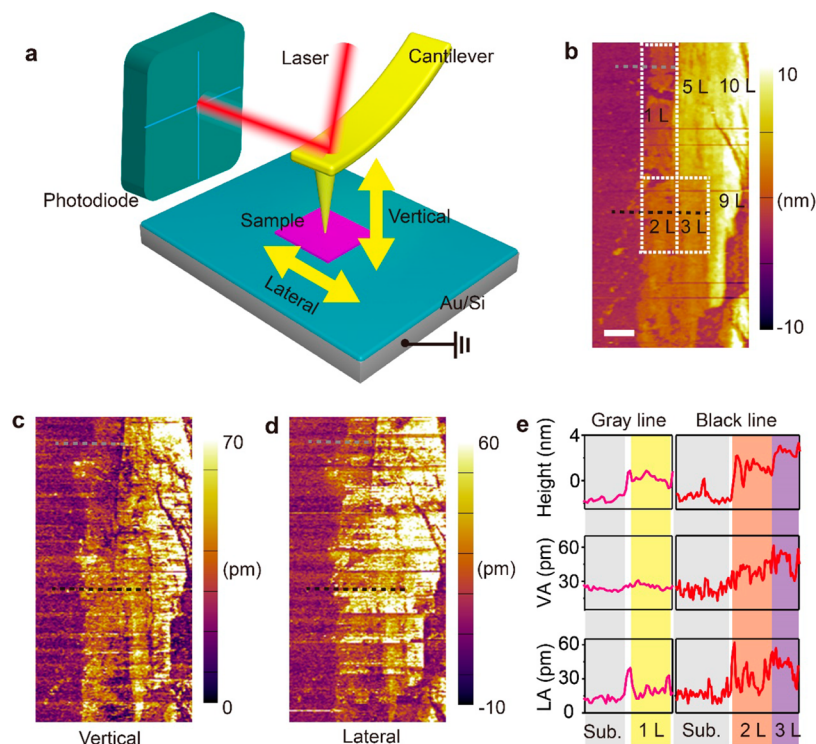
Figure 1. Existence of out-of-plane (vertical) and in-plane (lateral) piezoelectricity in monolayer, bilayer, and trilayer α-In$_2$Se$_3$. (a) Schematics of dual AC resonance tracking technique used in this work. The vertical and lateral vibrations of an AFM probe can be used to detect out-of-plane and in-plane piezoelectricity in α-In$_2$Se$_3$ nanoflakes. (b) AFM image of an exfoliated α-In$_2$Se$_3$ flake containing layers with different thicknesses. The monolayer, bilayer, and trilayer α-In$_2$Se$_3$ flakes are highlighted by the white dashed lines. Scale bar: 500 nm. The vertical PFM (c) and lateral PFM (d) images of the α-In$_2$Se$_3$ sample. The applied AC drive voltage is always fixed at 3 V. (e) Height and quantitative piezoresponse profiles extracted from the gray and black lines in b–d. The notations of "VA", "LA", and "Sub." represent the extracted vertical, lateral PFM amplitude, and the noise signal of the substrates, respectively.

in-plane piezoelectricity, some buckled monolayer materials, such as InP and AlAs, are also anticipated to exhibit out-of-plane piezoelectricity.[6] However, they are not easily obtainable as they typically crystallize in a three-dimensional zinc blende structure in ambient conditions.[12] Recently, Lu *et al.* have created a Janus MoSSe structure and experimentally demonstrated the out-of-plane piezoelectricity in a monolayer form.[13]

Theoretical calculations have predicted that monolayer α-In$_2$Se$_3$ possesses piezoelectricity and ferroelectricity in both in-plane and out-of-plane orientations.[14,15] Recent studies have experimentally shown the ferroelectric switching of α-In$_2$Se$_3$ down to 6 nm;[16,17] however, the piezoelectricity of such material has not been fully elucidated yet. Here, we experimentally observe the out-of-plane and in-plane piezo-electricity in both monolayer and multilayer hexagonal α-In$_2$Se$_3$ nanoflakes using piezoresponse force microscopy (PFM). We also uncover the layer-dependent out-of-plane and in-plane piezoelectric characteristics associated with substrate clamping effect. The d_{33} piezoelectric coefficient for monolayer α-In$_2$Se$_3$ is about 0.34 pm/V, and that for bulk evolves to 5.6 pm/V. Utilizing multilayer α-In$_2$Se$_3$, we successfully develop a flexible piezoelectric nanogenerator (PENG), which can produce the peak current and voltage of 47.3 pA and 35.7 mV, respectively, under the strain value of 0.76%. Our demonstration of highly flexible and transparent PENG based on α-In$_2$Se$_3$ has shown its potential application in bimechanical energy harvesting and electronic skin.

RESULTS AND DISCUSSION

Dual AC resonance technique (DART)-based PFM is used to characterize the piezoelectric properties of α-In$_2$Se$_3$ nanoflakes (see section 3 in the Supporting Information for details). The vertical PFM (VPFM) mode uses the up−down deflections of an atomic force microscope (AFM) cantilever to detect the out-of-plane deformation of samples, and the lateral PFM (LPFM) mode utilizes the twisting motion of probes to detect the in-plane deformations, as schematically illustrated in Figure 1a. The α-In$_2$Se$_3$ nanoflakes are mechanically exfoliated from their bulk samples and transferred onto a conductive substrate[18,19] (Au/Si) for our PFM measurements. Raman spectroscopy was employed to effectively characterize the stable semiconducting α-In$_2$Se$_3$ crystal at room temperature (see Figure S1) as previously reported.[17,20] Figure 1b shows the contact-mode topography of a typically exfoliated α-In$_2$Se$_3$ nanoflake with different thicknesses (below 12 nm), where the monolayer, bilayer, and trilayer flakes are highlighted by the white dashed lines. The corresponding VPFM and LPFM images are displayed in Figure 1c,d, respectively. Note that the PFM amplitudes in Figure 1c,d are the amplified values under the measuring condition of DART and not the actual piezoelectric responses; however, these results still allow us to conclude the piezoelectric behaviors qualitatively. The presented amplitude signals from both VPFM and LPFM highly coincide with the sample surface topography, demonstrating that the out-of-plane and in-plane piezoelectric responses come from the cleaved α-In$_2$Se$_3$ nanoflake.
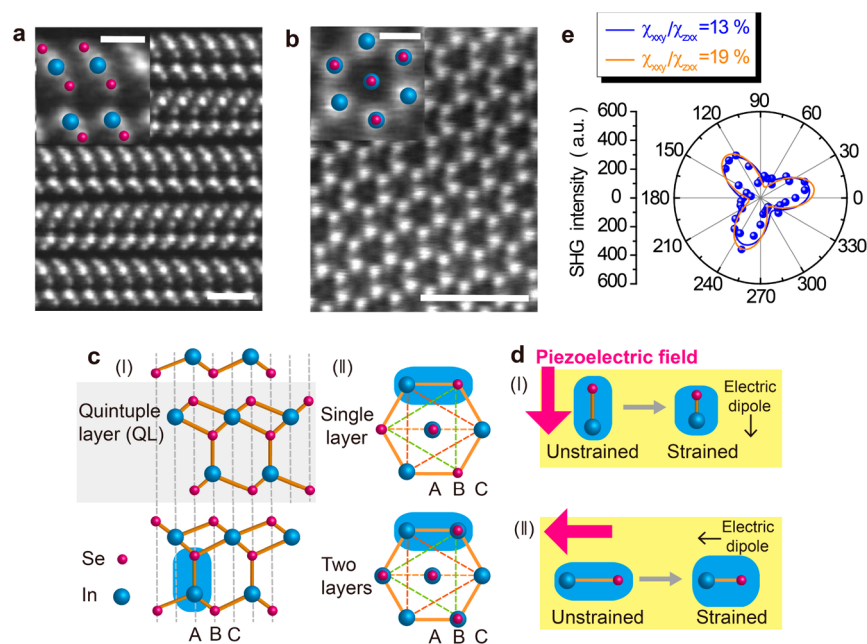
Figure 2. Structural analysis of the origin of out-of-plane and in-plane piezoelectricity in α-In$_2$Se$_3$ nanoflakes. Cross-sectional (a) and top-view (b) high-resolution STEM images of few-layer α-In$_2$Se$_3$ specimens. The insets show their corresponding enlarged images. Scale bar: 1 nm for the two large images, 350 pm for the inset in (a), and 180 pm for the inset in (b). (c) Proposed atom structure models for the side (I) and top (II) views of hexagonal α-In$_2$Se$_3$, indicating the pronounced noncentrosymmetric structure. (d) In the presence of externally vertical or lateral strain, the piezoelectric field resulting from cation and anion shift-induced electric dipole will occur along the pink arrows at the out-of-plane (I) or in-plane (II) direction. (e) Second harmonic generation (SHG) signals as a function of sample azimuthal angle θ for a multilayer α-In$_2$Se$_3$. The blue and yellow curves are used to fit with the raw data. The presented C_3 symmetry and large susceptibility tensor ratio of χ_{xxy} and χ_{zxx} indicate the coexistence of out-of-plane and in-plane noncentrosymmetry.

To further gain insight into the electromechanical responses from the monolayer, bilayer, and trilayer α-In$_2$Se$_3$ flakes, we extracted the data from the gray and black dashed lines in Figure 1b−d and plotted the corresponding profiles of height, vertical amplitude (VA), and lateral amplitude (LA) in Figure 1e, where the gray area shows the noise level of the substrate. The thickness of the monolayer, bilayer, and trilayer α-In$_2$Se$_3$ is about 1.5, 2.7, and 3.9 nm, respectively, and the average quintuple layer thickness is 1.2 nm, agreeing with the reported thickness of ∼1 nm.[16,20] The fluctuation in the height profile may be caused by the scratched samples when the AFM tip scans the surface back and forth in a contact mode. The consistent change in the vertical and lateral piezoelectric signals for the monolayer, bilayer, and trilayer α-In$_2$Se$_3$ strongly validate the presence of the in-plane and out-of-plane piezoelectricity. It should be emphasized that the piezoelectricity exists at an atom level, which intrinsically originates from the noncentrosymmetry in a unit cell crystal structure.

The atomic arrangement and structure of α-In$_2$Se$_3$ monolayers have been theoretically reported, and such asymmetry is proposed to exhibit ferroelectric properties.[15] Based on the atomic model, in-plane and out-of-plane piezoelectricity at a monolayer level is anticipated. When the monolayers stack together, α-In$_2$Se$_3$ may adopt two different structures: hexagonal and rhombohedral.[21,22] Our extensive structure characterizations by scanning transmission electron microscopy (STEM) and X-ray diffraction (XRD) (Figures 2a,b and S2) conclude that the crystal used in this work agrees with the hexagonal structure and $P6_3/mmc$ symmetry. For clarification, we summarize the differences of the two α-In$_2$Se$_3$ structures and propose a possible Raman peak located at

90 cm^{-1} to identify hexagonal or rhombohedral structure in section 2 of the Supporting Information.

Figure 2a,b shows the cross-sectional and top-view STEM images for a few-layer α-In$_2$Se$_3$, where the inset in each figure shows the magnified image with a high spatial resolution. The corresponding side-view and top-view illustrations for atomistic arrangements and crystal structures are displayed in Figure 2c. It is clear that the central Se layer is tetrahedrally sandwiched by two neighboring indium atoms, whereas the selenide atoms at the top and bottom surface layer regularly fill in the side hollow sites of the indium atoms. As seen from the STEM image or structure model, one quintuple layer is constituted by the alternately arranged Se−In−Se−In−Se atomic planes, where the indium and selenide atoms follow the repeated simple arrangement of ABC, as shown in Figure 2c(I). In addition, each neighboring quintuple layer keeps a constant dislocation along the horizontal direction, as the gray dashed lines indicate. Noticeably, this primary structure at any thickness always lacks the centrosymmetric property and provides the basic understanding for the generation of out-of-plane (d_{33}) piezoelectricity. When suffering an externally compressed force in the d_{33} direction, the α-In$_2$Se$_3$ crystal will immediately produce charged inner electric dipoles associated with the displacement of cation indium and anion selenide. The electric field triggered by those downward pointed electric dipoles will be further superimposed along the polarized direction (d_{33}), macroscopically resulting in the out-of-plane piezoelectric field as the pink arrow shows in Figure 2d(I). As illustrated in the top panel of Figure 2c(II), the atomic arrangement "ABC" in a single layer gives a basic hexagonal in-plane projection with each type of atoms arranged in a triangular lattice at the six vertexes. Because of the nonequivalent sites for the two Se atoms and one In
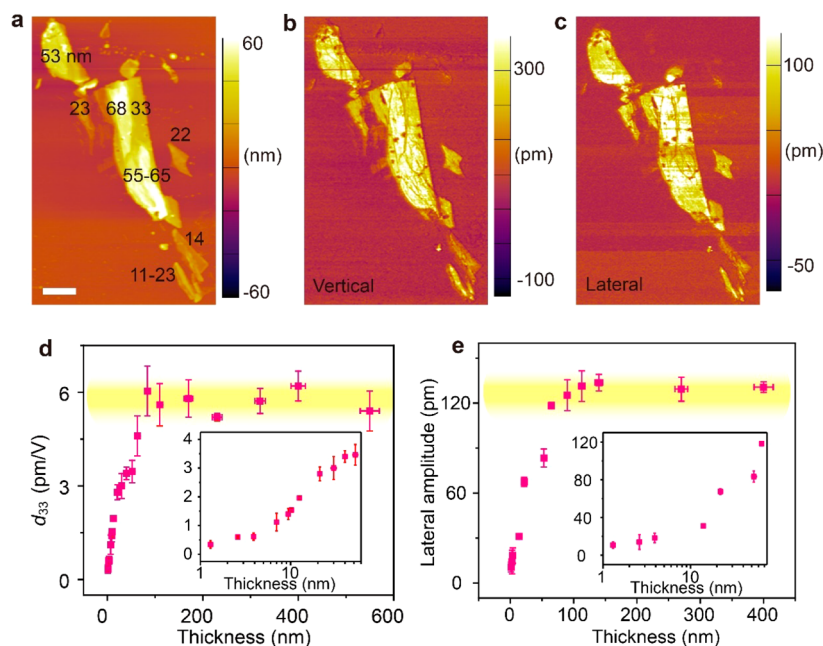
Figure 3. Evolution of the out-of-plane and in-plane piezoresponses with respect to the sample thickness. (a–c) AFM, vertical PFM, and lateral PFM images for a thick (>9L) α-In$_2$Se$_3$ sample. The detailed thickness is labeled in the AFM image. Scale bar: 5 μm. (d) Thickness dependence of the d_{33} piezoelectric coefficient. The inset image shows the enlarged changing relationship between d_{33} coefficient and thickness less than 60 nm. The d_{33} piezoelectric coefficient for the monolayer α-In$_2$Se$_3$ crystal is about 0.3 pm/V, and that for thick samples (>90 nm) will be eventually saturated at 5.6 pm/V. (e) Lateral amplitude (piezoresponse) as a function of α-In$_2$Se$_3$ thickness. The inset displays an enlarged image of less than 60 nm. It also presents a saturated trend when the thickness reaches ~90 nm. The horizontal and vertical error bars represent the standard deviations of sample thickness and piezoelectric response. Note that the background noise has been deducted for all the presented data here.

atom, such a hexagonal structure also evidently lacks the centrosymmetry. The charged electric dipole can emerge upon a planar strain, giving rise to the in-plane (d_{11}) piezoelectric field as the pink arrow displays (the bottom panel of Figure 2d(II)).

Interestingly, bilayer α-In$_2$Se$_3$ is exactly constructed by two dislocated quintuple layer and its in-plane projection contains two classes of atoms at the vertex of the hexagonal structure: Se−In−Se−Se and In−In (the bottom panel of Figure 2c(II)), leading to the noncentrosymmetry. Regarding the other thickness, the piezoelectric case is similar to that in monolayer or bilayer due to the repeated structure. Hence, the out-of-plane and in-plane piezoelectricity in hexagonal α-In$_2$Se$_3$ flakes always exists regardless of sample thickness. This is in clear contrast to the TMDC family with obvious odd−even layer number dependency (Figure S5). Finally, we employed second-harmonic generation (SHG) measurement to confirm that the origin of the observed piezoelectricity results from the out-of-plane and in-plane noncentrosymmetry of hexagonal α-In$_2$Se$_3$. Based on the theoretical calculation,[14] we can extract each component of the susceptibility tensor (in-plane χ_{xxy}; out-of-plane χ_{zxx} and χ_{zzz}) and get their correlated ratio, as shown in Figures 2e and S8. The nonzero ratio and polarized SHG signal reveal the broken inversion symmetry in the crystal's out-of-plane and in-plane orientations, which agrees with our stated structural analysis above.

The question whether the thick samples could remain the observed piezoelectricity motivated us to study the crystal with a thickness greater than 12 nm, as shown in Figure 3a−c. The PFM images display strong electromechanical responses, demonstrating the existence of inherently out-of-plane and in-plane piezoelectricity in thick and even bulk samples. Notably,

both vertical and lateral PFM responses present different amplitudes as the sample thickness varies. The d_{33} piezoelectric coefficient along the vertical orientation is derived from the relationship between the cantilever deflection and applied drive voltage and plotted as a function of thickness, as indicated in Figure 3d (for more details, see the Experimental Methods and Figure S6). Significantly, the d_{33} values for the monolayer and bilayer are 0.34 and 0.6 pm/V, respectively, consistent with those in the theoretical work.[14] With the thickness exceeding 90 nm, the related piezocoefficient will sequentially increase to a saturated value of 5.6 pm/V. As displayed in Figure S8, the result of SHG measurement also coincides with our observed increasing behavior. In addition, we still discovered this increased piezoelectric response with respect to the sample thickness in nonconductive silica substrates, indicating that this trend is not caused by an artifact such as the electron tunneling effect between the AFM tip and conductive substrate (Figure S9). The increase of piezoelectric response with thickness is virtually observed in some conventional or layered ferroelectric materials and piezoelectric biomolecules, which has been attributed to the decreased substrate constraint.[3,18,23]

For comparison, we proceeded to examine the synthesized β-In$_2$Se$_3$ via a physical vapor deposition (PVD) method and did not acquire any obvious PFM responses (Figure S10) owing to its face-centered cubic structure (centrosymmetry), confirming the discrepancy between α-In$_2$Se$_3$ and β-In$_2$Se$_3$. In addition, we also conducted the PFM characterization for monolayer WSe$_2$ to verify that the LPFM response shall not trigger the generation of a VPFM signal (Figure S11), further validating the accuracy of the in-plane piezoelectric measurement (LPFM). Note that the newly developed configuration of a suspended membrane with two terminals metallized can be
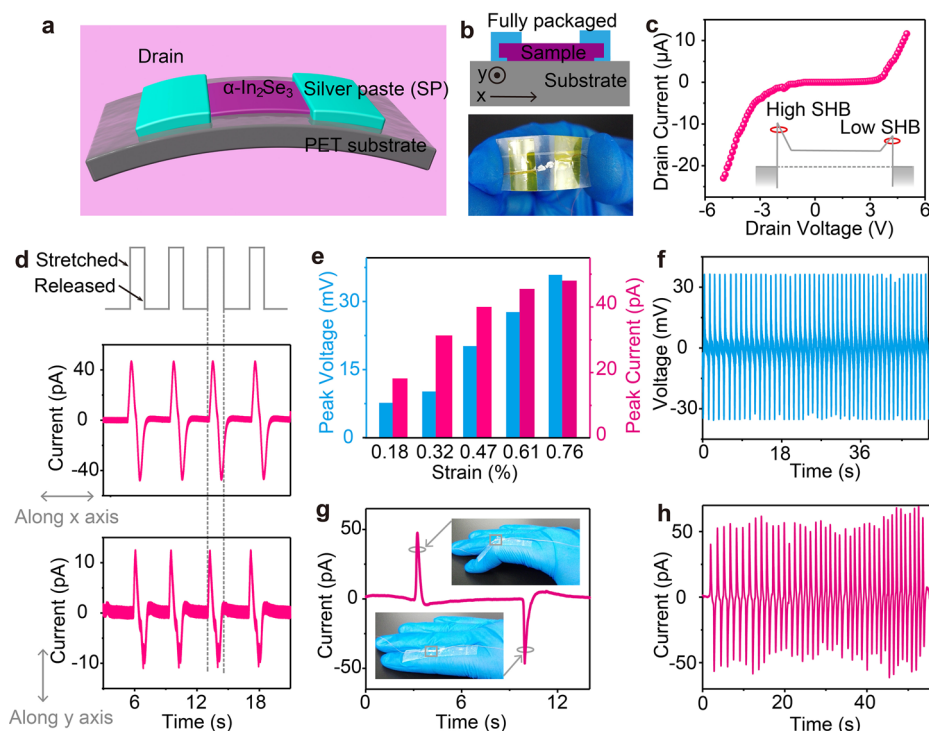
Figure 4. Piezoelectric outputs from multilayer α-In$_2$Se$_3$ nanogenerators. (a) Sketch of the flexible piezoelectric nanogenerators. (b) Side view of the sketched devices in (a). The α-In$_2$Se$_3$ semiconductors are fully encapsulated by silver paste. The x and y axes are defined as the directions parallel and normal with the long side of substrate, respectively. The bottom inset shows the optical graph of a typical α-In$_2$Se$_3$ piezoelectric nanogenerator. (c) Electrical output curve for the α-In$_2$Se$_3$ device. The sample and metal electrode obviously form good Schottky contacts. (d) Short-circuit current response of the α-In$_2$Se$_3$ nanogenerator under periodic strain (0.76%) in two different directions. (e) Strain dependence of the piezoelectric output (mean value from 10 replicates). (f) Typical open-circuit voltage outputs upon a strain value of 0.76%. (g) An α-In$_2$Se$_3$ piezoelectric nanogenerator is integrated on an index finger to scavenge the mechanical energy induced by finger motions. (h) Current outputs when the index finger repeatedly curves and extends.

used to accurately measure in-plane piezoelectric coefficient for 2D materials,[7] the basis of which is to transform the bias-voltage-induced in-plane strain of the sample to the detectable out-of-plane strain by AFM probes (Figure S7). The method is able to be used in a piezoelectric material with only lateral but not vertical piezoelectric responses. Due to the strong coupling of two perpendicularly orientated piezoelectricity in bent and suspended α-In$_2$Se$_3$ flakes, the accurate determination of their lateral piezoelectric coefficients (d_{11}) is not possible. However, the quantitative LPFM amplitude dependence on the sample thickness is still observed (Figure 3e). Similar to the out-of-plane piezoelectric behaviors, the in-plane piezoresponses first show an increasing trend and then exhibit a saturated level as the thickness reaches 90 nm. This highly intercorrelated change for both in-plane and out-of-plane piezoelectric behaviors should be ascribed to the decreasing substrate clamping effect as the tested thickness increases.[3,18,23] In summary, we can conclude that this hexagonal α-In$_2$Se$_3$ preserves the out-of-plane and in-plane piezoelectricity, irrespective of its thickness.

Recently, nanoscale piezoelectric-material-based electronics or energy-harvesting cells, such as nanogenerators, have drawn great attention due to the potential applications in active self-powered systems, wireless transmission, and human interfacing.[8,24−31] We have demonstrated a type of flexible α-In$_2$Se$_3$ piezoelectric nanogenerator. Multilayer samples with thicknesses of 100−200 nm are transferred to the polyethylene terephthalate (PET) substrates for PENG fabrication (Figure 4a). Silver paste is used as the two metal electrodes. Due to the fluidity of silver paste, two terminals of the multilayer α-In$_2$Se$_3$

are often fully encapsulated, as shown at the top of Figure 4b, which will be beneficial to exploit the vertical and lateral polarization charges for the piezoelectric outputs. We define the x axis as the length direction of the substrate and the y axis as the width direction. Optical graph of a typically flexible and transparent PENG is shown at the bottom panel of Figure 4b. Electrical measurement in Figure 4c shows that both metal−semiconductor junctions of the PENG are Schottky contacts (Figure 4 and details in Figure S12), which are crucial for the piezoelectric outputs.[32,33]

Figure 4d shows the piezoelectric current responses of the as-fabricated PENG. Periodic strains were applied to the devices using a commercially linear motor system. When the strain is applied on the x or y direction, positive current output is observed with increasing strain, and negative output can be seen with the decreasing strain, directly verifying the existence of piezoelectricity and the conversion of mechanical energy into electricity. Noticeably, in this device configuration, the coupling of in-plane and out-of-plane piezoelectricity in α-In$_2$Se$_3$ flakes facilitates the PENG working at any applied strain direction. As indicated in Figure 4e, both the piezoelectric outputs (peak voltage and peak current) increase with the magnitude of applied strain increased. A stable voltage signal under a fixed (0.76%) and short strain interval of 1 s is displayed in Figure 4f, demonstrating excellent output reproducibility. Note that the PENG can give the voltage and current output of 35.7 mV and 47.3 pA, respectively, at 0.76% strain, which corresponds to the charge value of 17.5 pC. Additionally, a connection polarity reversion test is performed to show that an output voltage

signal will be expectedly reversed when the connection polarity is switched, confirming that the electrical outputs come from PENG and not from some other factors (Figure S13). The stability of the PENG has been examined by repeatedly stretching−releasing a device for 35 min (Figure S14). As previously reported,[34] the defects, such as sulfur vacancies or intercalations in α-In$_2$Se$_3$, can affect the piezoelectric performance of the as-fabricated devices through carrier screening effects. The defect-dependent piezoelectric outputs for this material need future systematical investigations. Furthermore, for integrating the PENG onto human skin, such as the back of an index finger, we changed the PET substrate to highly flexible and transparent common "scotch" tape. Once the index finger adhered to the as-fabricated PENG does a curving or extending motion, the device can immediately give a peak current response (Figure 4g). When the index finger continuously curves and extends, the PENG shall incessantly output current and voltage signals, as shown in Figures 4h and S15, demonstrating that this type of device has great potential for harvesting bimechanical energy or acting as electronic skin.

CONCLUSIONS

In conclusion, we show evidence of the coexistence of out-of-plane and in-plane piezoelectricity in both monolayer and multilayer α-In$_2$Se$_3$ using PFM. We investigate the layer-dependent out-of-plane and in-plane piezoelectric responses: with the thickness increased, the vertical and lateral piezosignals dramatically increase and then reach saturated values. Specifically, the d_{33} piezoelectric coefficient is 0.34 pm/V for monolayer α-In$_2$Se$_3$ and 5.6 pm/V for bulk crystal. Moreover, we develop a multilayer α-In$_2$Se$_3$-based piezoelectric nanogenerator with output current and voltage of 35.7 mV and 47.3 pA, respectively, at 0.76% strain and demonstrate its application in electronic skin and bimechanical energy harvesting. The piezoelectric device made from the hexagonally stacked α-In$_2$Se$_3$ flakes offers an opportunity to enable piezoelectric devices responding to strain from all directions.

EXPERIMENTAL METHODS

Preparation of the α-In$_2$Se$_3$ Nanoflakes. The synthesized bulk α-In$_2$Se$_3$ crystal was bought from a 2D semiconductor company. Before being exfoliated, the Au (60 nm)/Si or SiO$_2$ (300 nm)/Si substrate was first treated by O$_2$ plasma at 80 W for about 5 min in order to clean the substrate and enhance the cleaved yield of atomic thin samples. For the exfoliating processes, we want to emphasize the following items that are important to obtain a high yield rate of atomic thin samples. When the two adhered scotch tapes were separated, tension force should be always applied, and an acute angle as small as possible should be kept between the tapes. In the transferring procedure from tape to the target substrate, the tape should be holding tension and flat to come close to the substrate. Once the tape and substrate adhere to each other, use the fingers to slightly press them to make them fully contacted. All the exfoliated α-In$_2$Se$_3$ nanoflakes were successively identified by their optical contrast and AFM.

Raman, PFM, TEM, and SHG Characterizations. The Raman measurement was conducted using an excitation laser of 532 nm (WITec alpha 300 confocal Raman microscopy). To avoid damaging the samples, we tuned the power density of the laser at a relatively small value, such as 10% of the total laser power. The PFM measurement was carried out on a Cypher ES-Asylum Research Oxford Instruments device using contact mode. A soft conductive tip with Pt/Ti coating and a spring constant of 2 N/m was employed in all PFM measurements. The α-In$_2$Se$_3$ crystals were transferred onto a holey carbon film supported on copper grids using a PMMA-mediated method. High-resolution scanning transmission electron microscopy

(Titan 60-300, FEI) was used to characterize the crystal structure of the samples. SHG measurement was conducted using a Ti:sapphire femtosecond-pulsed laser by a homemade optical microscope in the backscattering configuration. The polarization of fundamental and SH lights was selected in parallel conditions by individual linear polarizers. The sample was rotated azimuthally by a motorized rotational stage with 10° steps.

Calculating the d_{33} Piezoelectric Coefficient. The VPFM images for α-In$_2$Se$_3$ nanoflakes are used to qualitatively describe the out-of-plane piezoelectric response. We chose three or four different spots on the sample surface to quantitatively collect the piezoelectric response. To estimate the d_{33} value, the vertical deflection of the used AFM cantilever is a vital parameter. By multiplying the calibration of the inverse optical lever sensitivity (InvOLS) with the deflection signals, the amplitude (unit: pm) of the tip motion can be derived. The calibration constant was obtained from the slope of the force−distance curve. During the process of piezoelectric measurement, the applied electric field between the AFM tip and conductive substrate is always nonuniform. Hence, we can only obtain the effective piezoelectric coefficient (d_{eff}) from the slope of drive voltage and amplitude as the following equation shows.

$$A_{\text{f}} = V_{\text{f}} \times \delta = Q d_{\text{eff}} \times U_{\text{f}}$$

in which A_{f} is the amplitude (in unit of nm), V_{f} is vertical deflection signal (in unit of mV), δ is the calibration constant of InvOLS (nm/V), U_{f} represents the applied AC drive voltage (V), and Q is the quality factor.

In the case of weak indentation, where the indentation of the AFM tip into the sample is less than the tip radius (∼25 nm) in this work, the values of d_{33} and d_{eff} approximately follow the equation: $d_{33} = 2 \times d_{\text{eff}}$.[35,36] From this relationship, we can estimate the d_{33} piezoelectric coefficient for α-In$_2$Se$_3$ flakes.

Fabrication of the Piezoelectric Nanogenerator. The α-In$_2$Se$_3$ nanoflakes with typical thickness and size of 100−200 nm and 50−100 μm are chosen as the basic building block of the PENGs. The used PET flexible substrate is about 500 μm thick. The PET substrate was first cleaned by acetone, isopropyl alcohol, and deionized water to avoid a substrate-induced doping effect in the α-In$_2$Se$_3$ nanoflakes. Then, the PET was dried by nitrogen gas and baking at 80 °C for 20 min. Next, the identified α-In$_2$Se$_3$ nanoflakes were transferred onto the pretreated PET substrate using a PMMA-assisted wet chemical method. The silver paste was dripped on the two sides of the samples under an optical microscope to act as the electrodes. Generally, the channels between two electrodes were about 30−60 μm in length and 20−100 μm in width. The intrinsic coupling of out-of-plane and angle-dependent in-plane piezoelectricity in α-In$_2$Se$_3$ nanoflakes always exists regardless of the strain direction. Therefore, in the fabricating procedures, we do not need to pay attention to the orientation between electrodes and crystal symmetry as in the case of monolayer MoS$_2$.[8]

Characterization of the Piezoelectric Output. A low-noise current preamplifier (SR570, Stanford Research Systems) and a low-noise voltage preamplifier (SR560) were used to measure current and voltage signals, respectively. A 3 Hz low-pass filter and a band-pass filter (0.1−10 Hz) were used for both current and voltage measurements. A home-built software programmed by Labview was used to collect and record the data. A Lin motor was used for applying the strain on the devices. When the PENG was tested, one end of the as-fabricated devices was clamped on the optical table, and the other end acted as a free terminal for applying external force by the Lin motor.

Estimation of the Magnitude of Strain in α-In$_2$Se$_3$ Devices. The dimension of α-In$_2$Se$_3$ nanoflakes is far smaller than that of the PET substrate (3.5 cm × 1.5 cm × 500 μm), and the mechanical response of the whole device will be affected by the substrate, not the samples. The related strain (ε) can be estimated by the following equation:[8]

$$\varepsilon = 3 \frac{a}{2l} \frac{D_{\text{max}}}{l} \left(1 - \frac{z_0}{l} \right)$$

where a and l depict the thickness and length of the PET substrate, z_0 represents the distance between the fixed edge and the α-In$_2$Se$_3$ nanoflake, and D_{max} is the lateral shift of the free end of the substrate.

ASSOCIATED CONTENT

⑤ Supporting Information

The Supporting Information is available free of charge on the ACS Publications website at DOI: 10.1021/acsnano.8b02152.

Raman characterization of the α-In$_2$Se$_3$ crystal, XRD and electron diffraction patterns of the bulk α-In$_2$Se$_3$ crystal, crystal structure models for rhombohedral and hexagonal α-In$_2$Se$_3$, resonance frequencies for the vertical and lateral piezoelectric measurement, interpretation of the evolution of piezoelectric effect in 2H monolayer and bilayer WSe$_2$ crystals, out-of-plane piezocoefficient estimation of α-In$_2$Se$_3$ crystals, schematics of measuring the in-plane piezocoefficient in 2D materials, SHG intensity as a function of sample thickness, silica substrate based vertical piezocoefficients as a relation of thickness, piezo responses for β-In$_2$Se$_3$ crystals synthesized by PVD method with thickness of 1 and 9 nm, piezo responses for CVD synthesized monolayer WSe$_2$, underlying physical mechanism of piezoelectric output in α-In$_2$Se$_3$ nanogenerator, voltage outputs for the α-In$_2$Se$_3$ crystal based piezoelectric nanogenerator with connection polarity reversed, periodic test showing the stability of a α-In$_2$Se$_3$ piezoelectric nanogenerator upon strain value of 0.18%, voltage outputs when the index-finger repeatedly bends and straightens, and summary of the typical Raman peaks of α-In$_2$Se$_3$ (PDF)

AUTHOR INFORMATION

Corresponding Authors
*E-mail: xixiang.zhang@kaust.edu.sa.
*E-mail: ljliv@tsmc.com.

ORCID ⓘ
Weijin Hu: 0000-0001-5862-1481
Jr-Hau He: 0000-0003-1886-9241
Zhong Lin Wang: 0000-0002-5530-0380
Xixiang Zhang: 0000-0002-3478-6414
Lain-Jong Li: 0000-0002-4059-7783

Author Contributions
▼F.X. and J.Z. contributed equally.

Notes
The authors declare no competing financial interest.

REFERENCES

(1) Wang, Z. L.; Song, J. H. Piezoelectric Nanogenerators Based on Zinc Oxide Nanowire Arrays. *Science* **2006**, *312*, 242−246.

(2) Chang, C. E.; Tran, V. H.; Wang, J. B.; Fuh, Y. K.; Lin, L. W. Direct-Write Piezoelectric Polymeric Nangenerator with High Energy Conversion Efficiency. *Nano Lett.* **2010**, *10*, 726−731.

(3) Lee, B. Y.; Zhang, J. X.; Zueger, C.; Chung, W. J.; Yoo, S. Y.; Wang, E.; Meyer, J.; Ramesh, R.; Lee, S. W. Virus-Based Piezoelectric Energy Generation. *Nat. Nanotechnol.* **2012**, *7*, 351−356.

(4) Kingon, A. I.; Srinivasan, S. Lead Zirconate Titanate Thin Films Directly on Copper Electrodes for Ferroelectric, Dielectric and Piezoelectric Applications. *Nat. Mater.* **2005**, *4*, 233−237.

(5) Bruant, I.; Gallimard, L.; Nikoukar, S. Optimal Piezoelectric Actuator and Sensor Location for Active Vibration Control Using Genetic Algorithm. *J. Sound Vib.* **2010**, *329*, 1615−1635.

(6) Blonsky, M. N.; Zhuang, H. L. L.; Singh, A. K.; Hennig, R. G. Ab Initio Prediction of Piezoelectricity in Two-Dimensional Materials. *ACS Nano* **2015**, *9*, 9885−9891.

(7) Duerloo, K. A. N.; Ong, M. T.; Reed, E. J. Intrinsic Piezoelectricity in Two-Dimensional Materials. *J. Phys. Chem. Lett.* **2012**, *3*, 2871−2876.

(8) Wu, W. Z.; Wang, L.; Li, Y. L.; Zhang, F.; Lin, L.; Niu, S. M.; Chenet, D.; Zhang, X.; Hao, Y. F.; Heinz, T. F.; Hone, J.; Wang, Z. L. Piezoelectricity of Single-Atomic-Layer MoS$_2$ for Energy Conversion and Piezotronics. *Nature* **2014**, *514*, 470−474.

(9) Qi, J. J.; Lan, Y. W.; Stieg, A. Z.; Chen, J. H.; Zhong, Y. L.; Li, L. J.; Chen, C. D.; Zhang, Y.; Wang, K. L. Piezoelectric Effect in Chemical Vapour Deposition-Grown Atomic-Monolayer Triangular Molybdenum Disulfide Piezotronics. *Nat. Commun.* **2015**, *6*, 7430.

(10) Michel, K. H.; Verberck, B. Phonon Dispersions and Piezoelectricity in Bulk and Multilayers of Hexagonal Boron Nitride. *Phys. Rev. B: Condens. Matter Mater. Phys.* **2011**, *83*, 115328.

(11) Zhu, H. Y.; Wang, Y.; Xiao, J.; Liu, M.; Xiong, S. M.; Wong, Z. J.; Ye, Z. L.; Ye, Y.; Yin, X. B.; Zhang, X. Observation of Piezoelectricity in Free-Standing Monolayer MoS$_2$. *Nat. Nanotechnol.* **2015**, *10*, 151−155.

(12) Longo, R. C.; Carrete, J.; Alemany, M. M. G.; Gallego, L. J. Electronic Properties of Pure and p-type Doped Hexagonal Sheets and Zigzag Nanoribbons of InP. *J. Phys.: Condens. Matter* **2013**, *25*, 085506.

(13) Lu, A. Y.; Zhu, H. Y.; Xiao, J.; Chuu, C. P.; Han, Y. M.; Chiu, M. H.; Cheng, C. C.; Yang, C. W.; Wei, K. H.; Yang, Y. M.; Wang, Y.; Sokaras, D.; Nordlund, D.; Yang, P. D.; Muller, D. A.; Chou, M. Y.; Zhang, X.; Li, L. J. Janus Monolayers of Transition Metal Dichalcogenides. *Nat. Nanotechnol.* **2017**, *12*, 744−749.

(14) Hu, L.; Huang, X. R. Peculiar Electronic, Strong In-Plane and Out-of-Plane Second Harmonic Generation and Piezoelectric Properties of Atom-Thick alpha-M$_2$X$_3$ (M = Ga, In; X = S, Se): Role of Spontaneous Electric Dipole Orientations. *RSC Adv.* **2017**, *7*, 55034−55043.

(15) Ding, W. J.; Zhu, J. B.; Wang, Z.; Gao, Y. F.; Xiao, D.; Gu, Y.; Zhang, Z. Y.; Zhu, W. G. Prediction of Intrinsic Two-Dimensional Ferroelectrics in In$_2$Se$_3$ and Other III$_2$-VI$_3$ Van Der Waals Materials. *Nat. Commun.* **2017**, *8*, 14956.

(16) Zhou, Y.; Wu, D.; Zhu, Y. H.; Cho, Y. J.; He, Q.; Yang, X.; Herrera, K.; Chu, Z. D.; Han, Y.; Downer, M. C.; Peng, H. L.; Lai, K. J. Out-of-Plane Piezoelectricity and Ferroelectricity in Layered alpha-In$_2$Se$_3$ Nanoflakes. *Nano Lett.* **2017**, *17*, 5508−5513.

(17) Cui, C.; Hu, W. J.; Yan, X.; Addiego, C.; Gao, W.; Wang, Y.; Wang, Z.; Li, L.; Cheng, Y.; Li, P.; Zhang, X.; Alshareef, H. N.; Wu, T.; Zhu, W.; Pan, X.; Li, L. J. Intercorrelated In-Plane and Out-of-Plane Ferroelectricity in Ultrathin Two-Dimensional Layered Semiconductor In$_2$Se$_3$. *Nano Lett.* **2018**, *18*, 1253−1258.

(18) Liu, F. C.; You, L.; Seyler, K. L.; Li, X. B.; Yu, P.; Lin, J. H.; Wang, X. W.; Zhou, J. D.; Wang, H.; He, H. Y.; Pantelides, S. T.; Zhou, W.; Sharma, P.; Xu, X. D.; Ajayan, P. M.; Wang, J. L.; Liu, Z. Room-Temperature Ferroelectricity in CuInP$_2$S$_6$ Ultrathin Flakes. *Nat. Commun.* **2016**, *7*, 12357.

(19) Zhao, M. H.; Wang, Z. L.; Mao, S. X. Piezoelectric Characterization of Individual Zinc Oxide Nanobelt Probed by Piezoresponse Force Microscope. *Nano Lett.* **2004**, *4*, 587−590.

(20) Zhou, J.; Zeng, Q.; Lv, D.; Sun, L.; Niu, L.; Fu, W.; Liu, F.; Shen, Z.; Jin, C.; Liu, Z. Controlled Synthesis of High-Quality Monolayered alpha-In$_2$Se$_3$ *via* Physical Vapor Deposition. *Nano Lett.* **2015**, *15*, 6400−5.

(21) Popovic, S.; Celustka, B.; Bidjin, D. X-Ray Diffraction Measurement of Lattice Parameters of In$_2$Se$_3$. *Phys. Status Solidi. A* **1971**, *6*, 301.

(22) Popovic, S.; Tonejc, A.; Grzetaplenkovic, B.; Celustka, B.; Trojko, R. Revised and New Crystal Data for Indium Selenides. *J. Appl. Crystallogr.* **1979**, *12*, 416−420.

(23) Kim, D. M.; Eom, C. B.; Nagarajan, V.; Ouyang, J.; Ramesh, R.; Vaithyanathan, V.; Schlom, D. G. Thickness Dependence of Structural and Piezoelectric Properties of Epitaxial $Pb(Zr_{0.52}Ti_{0.48})O_3$ Films on Si and $SrTiO_3$ Substrates. *Appl. Phys. Lett.* **2006**, *88*, 142904.

(24) Xu, S.; Qin, Y.; Xu, C.; Wei, Y. G.; Yang, R. S.; Wang, Z. L. Self-Powered Nanowire Devices. *Nat. Nanotechnol.* **2010**, *5*, 366−373.

(25) Yang, R. S.; Qin, Y.; Dai, L. M.; Wang, Z. L. Power Generation with Laterally Packaged Piezoelectric Fine Wires. *Nat. Nanotechnol.* **2009**, *4*, 34−39.

(26) Xu, S.; Hansen, B. J.; Wang, Z. L. Piezoelectric-Nanowire-Enabled Power Source for Driving Wireless Microelectronics. *Nat. Commun.* **2010**, *1*, 93.

(27) Zhang, Y.; Yan, X.; Yang, Y.; Huang, Y.; Liao, Q.; Qi, J. Scanning Probe Study on the Piezotronic Effect in ZnO Nanomaterials and Nanodevices. *Adv. Mater.* **2012**, *24*, 4647−55.

(28) Zhang, Y.; Yang, Y.; Gu, Y.; Yan, X.; Liao, Q.; Li, P.; Zhang, Z.; Wang, Z. Performance and Service Behavior in 1-D nanostructured Energy Conversion Devices. *Nano Energy* **2015**, *14*, 30−48.

(29) Zhang, Z.; Liao, Q.; Yu, Y.; Wang, X.; Zhang, Y. Enhanced Photoresponse of ZnO Nanorods-Based Self-Powered Photodetector by Piezotronic Interface Engineering. *Nano Energy* **2014**, *9*, 237−244.

(30) Xue, F.; Chen, L. B.; Chen, J.; Liu, J. B.; Wang, L. F.; Chen, M. X.; Pang, Y. K.; Yang, X. N.; Gao, G. Y.; Zhai, J. Y.; Wang, Z. L. p-Type MoS_2 and n-Type ZnO Diode and Its Performance Enhancement by the Piezophototronic Effect. *Adv. Mater.* **2016**, *28*, 3391−3398.

(31) Xue, F.; Yang, L. J.; Chen, M. X.; Chen, J.; Yang, X. N.; Wang, L. F.; Chen, L. B.; Pan, C. F.; Wang, Z. L. Enhanced Photoresponsivity of the MoS_2-GaN Heterojunction Diode *via* the Piezo-phototronic Effect. *NPG Asia Mater.* **2017**, *9*, e418.

(32) Lu, M. P.; Song, J.; Lu, M. Y.; Chen, M. T.; Gao, Y.; Chen, L. J.; Wang, Z. L. Piezoelectric Nanogenerator Using p-Type ZnO Nanowire Arrays. *Nano Lett.* **2009**, *9*, 1223−1227.

(33) Hu, Y. F.; Wang, Z. L. Recent Progress in Piezoelectric Nanogenerators as a Sustainable Power Source in Self-Powered Systems and Active Sensors. *Nano Energy* **2015**, *14*, 3−14.

(34) Xue, X. Y.; Nie, Y. X.; He, B.; Xing, L. L.; Zhang, Y.; Wang, Z. L. Surface Free-Carrier Screening Effect on the Output of a ZnO Nanowire Nanogenerator and Its Potential as a Self-Powered Active Gas Sensor. *Nanotechnology* **2013**, *24*, 225501.

(35) Wang, X. W.; He, X. X.; Zhu, H. F.; Sun, L. F.; Fu, W.; Wang, X. L.; Hoong, L. C.; Wang, H.; Zeng, Q. S.; Zhao, W.; Wei, J.; Jin, Z.; Shen, Z. X.; Liu, J.; Zhang, T.; Liu, Z. Subatomic Deformation Driven by Vertical Piezoelectricity from CdS Ultrathin Films. *Sci. Adv.* **2016**, *2*, e1600209.

(36) Kalinin, S. V.; Bonnell, D. A. Imaging Mechanism of Piezoresponse Force Microscopy of Ferroelectric Surfaces. *Phys. Rev. B: Condens. Matter Mater. Phys.* **2002**, *65*, 125408.